A study of $\gamma p \to K^* K^* p$ in the Meson Spectroscopy Facility at CEBAF

Curtis A. Meyer

May 29, 1998

Detector Response to $K^* \bar{K}^*$ Systems

Introduction

Reaction 1 has been used as a benchmark to examine both acceptance and kaon identification in the detector. Events have been generated according to phase-space with a t-dependence given as $e^{-\alpha|t|}$ with a slope parameter, $\alpha = 5$.

$$\gamma p \to p \left\{ X \to \left[\left(K^{*0} \to K^+ \pi^- \right) \left(\bar{K}^{*0} \to K^- \pi^+ \right) \right] \right\} \tag{1}$$

The resonance X has been taken with a width $\Gamma = 0.150 GeV$ decaying into $\bar{K}^* K^*$. Equal numbers of events for m_X of 1.7 GeV/c^2, 2.5GeV/c^2 and 3.2GeV/c^2 have been produced for photon beam energies of 8, 10 and 12 GeV, while for 6GeV, only the 1.7 GeV/c^2 and 2.5GeV/c^2 masses have been generated.

Chew-Low Plots

Figure 1 shows the Chew-Low plot, $\left| t \right|$ versus m_x^2, for the four beam energies. While all the plots are limited by the $K^* \bar{K}^*$ threshold at about 1.76GeV/c^2, the important feature in these plots is the right-hand side curved edge of the data. This rapid rise limits the mass range over which we can explore resonances. From these plots, we will be limited to about 2GeV/c^2 for 6GeV photons. The limit will increase by about 0.25GeV/c^2 for each additional GeV of beam energy, up to about 3.5GeV/c^2 at 12 GeV.

Figure: The -t versus m_x^2 distributions for the generated events at E_γ of 6, 8, 10 and 12 GeV.

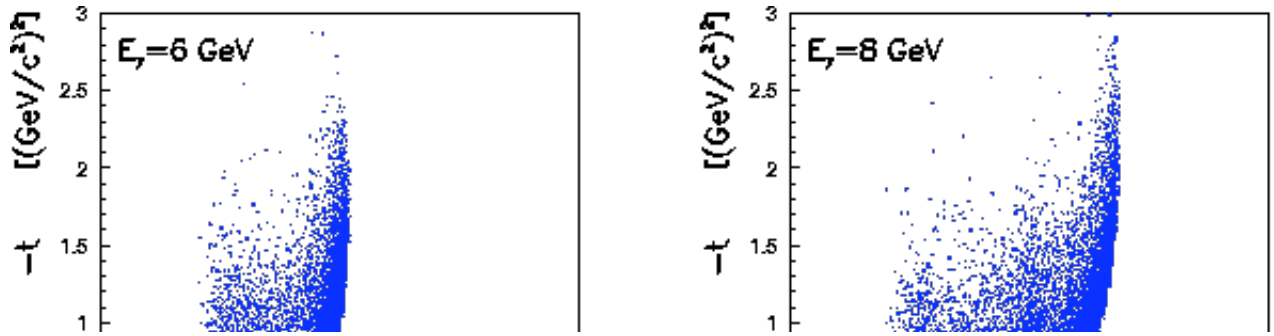

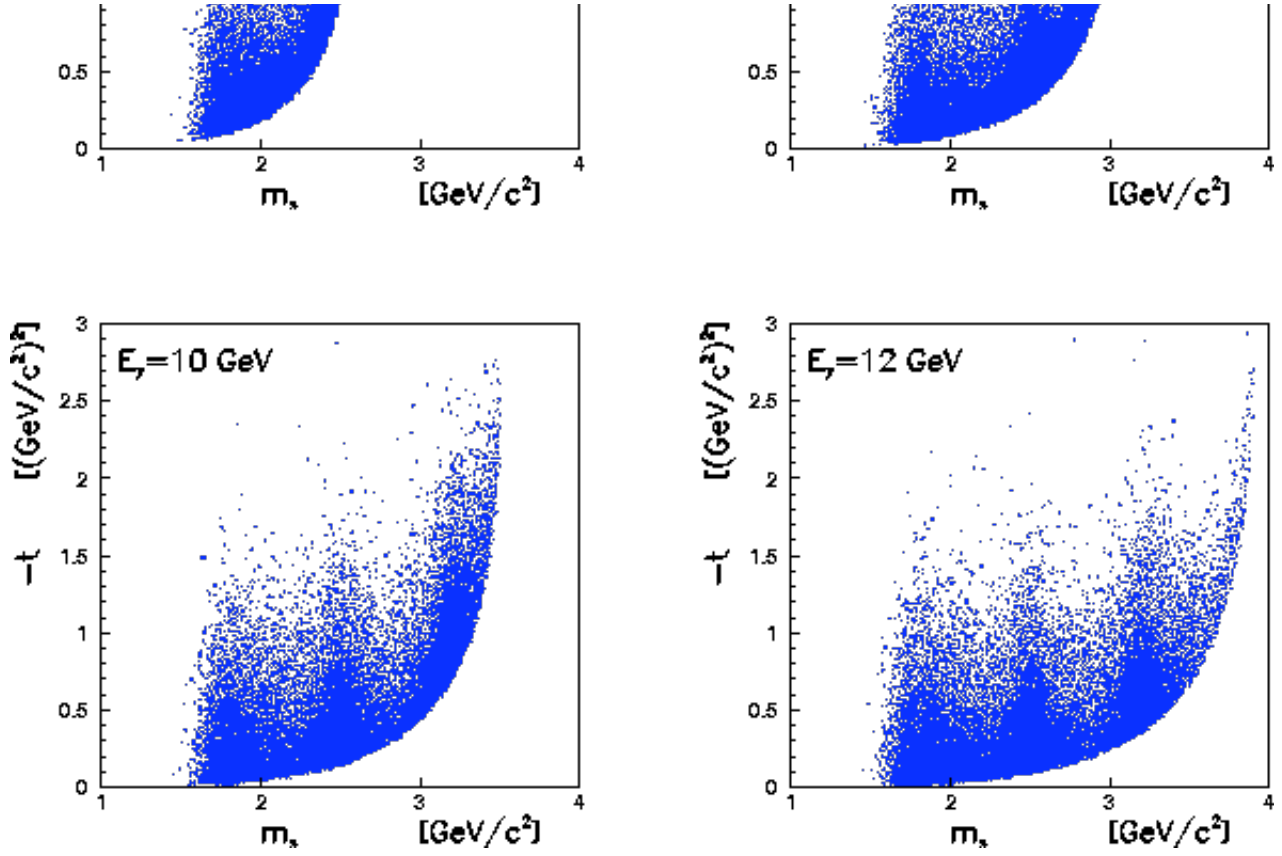

Dalitz Plots

Figure 2 shows the Dalitz plot for the same events as in Figure 1. We have assumed that we have cleanly identified the K^*'s, and have formed the K^*p invariant mass. The edges of these plots are a bit *soft* due to the width of the K^*. Again, we see the same limitations as before. In the 6GeV data, the 2.5GeV/c^2 band is pushed to the lower corner of the plot, and is likely to have strong interference over much of its angular distribution. While as we increase the beam energy, the plots expand and allow more access to these resonances.

Figure: The Dalitz plots for $K^{*\circ}p$ versus $\bar{K}^{*\circ}p$ for the four beam energies. The diagonal bands indicate the $K^{*\circ}\bar{K}^{*\circ}$ resonances in the simulated data.

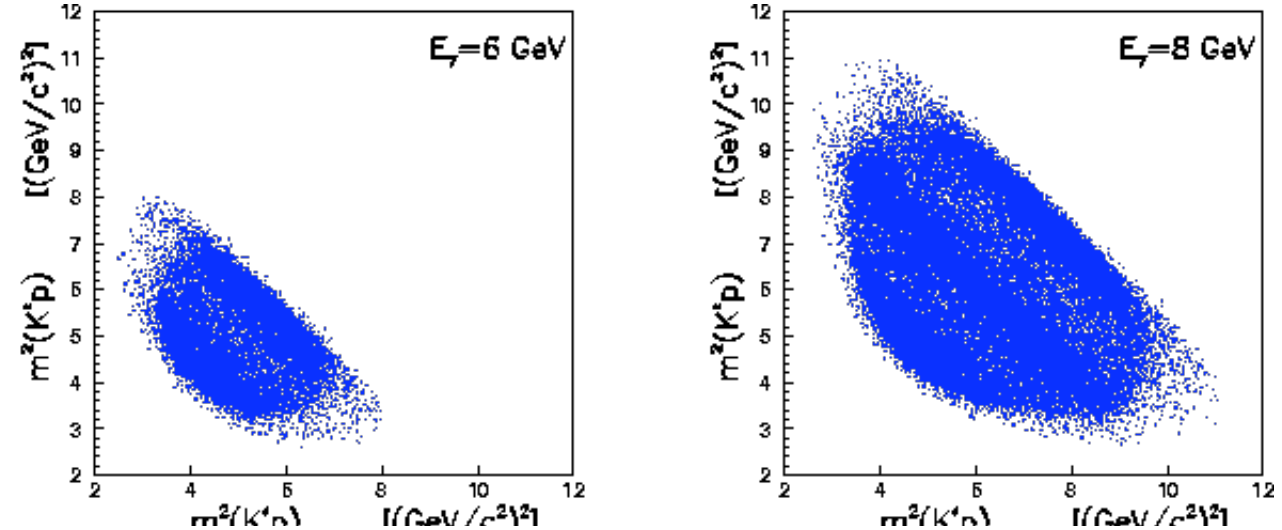

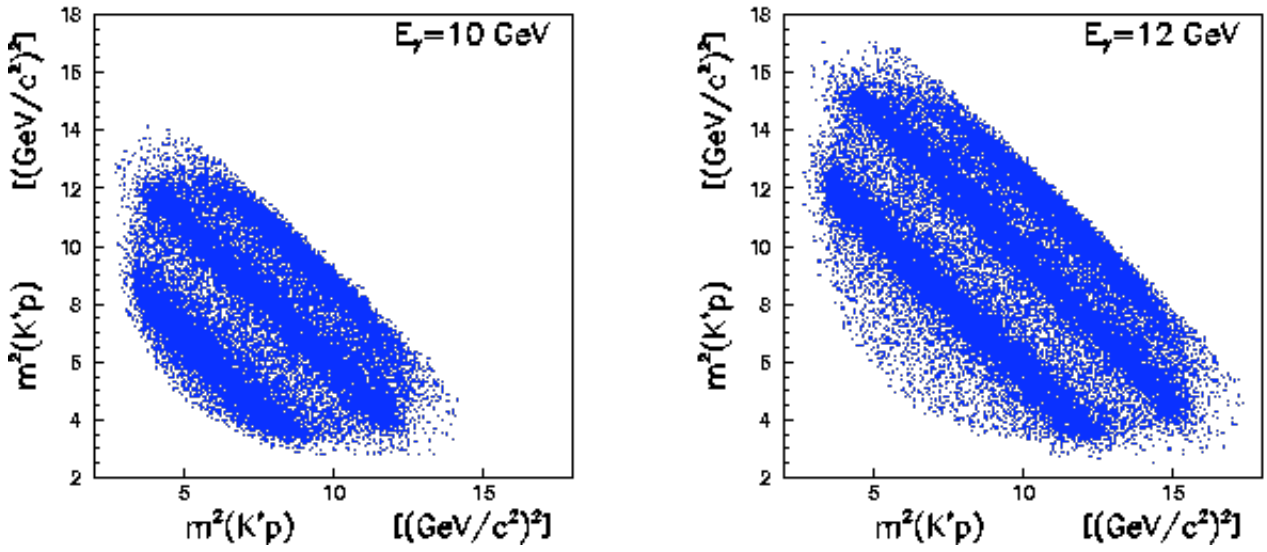

Acceptance for PWA

Another important issue in this is how is the acceptance for partial wave analysis affected by cuts dues to acceptance of the detector system. We will examine this both in terms of the invariant mass of the $K^*\bar{K}^*$ system, and the $\cos(\theta_{GJ})$,where θ_{GJ} is the Godfreid-Jackson angle for the $K^*\bar{K}^*$ system. It should be pointed out that these results are dependent upon the exact channel of interest and are only given as an illustrative example. In Figure 3 is plotted the $\bar{K}^*K^*$ invariant mass at $E_\gamma = 8GeV$ for all events, and for cuts on three different scattering angles, θ. In Figure 4 we have taken the plots as in Figure 3 and formed efficiencies as a function of the invariant mass. This has been done for all four beam energies.

Figure: The reconstructed $\bar{K}^*K^*$ invariant mass for an $8GeV$ photon beam as a function of the most forward scattering angle which can be reconstructed. **a** is for all events, **b** is for θ larger than 2°, **c** is for θ larger than 5° and **d** is for θ large than 8°

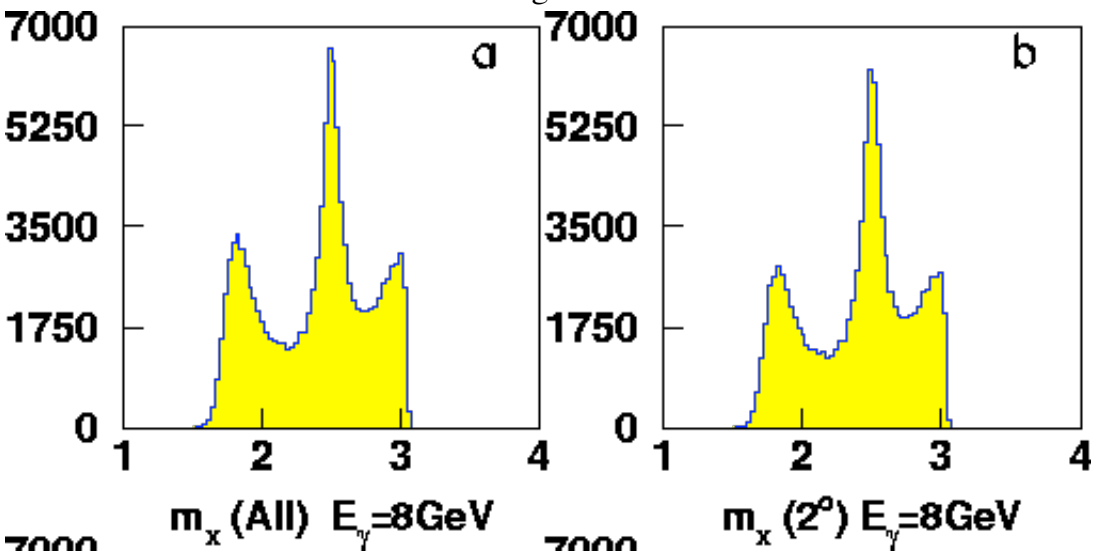

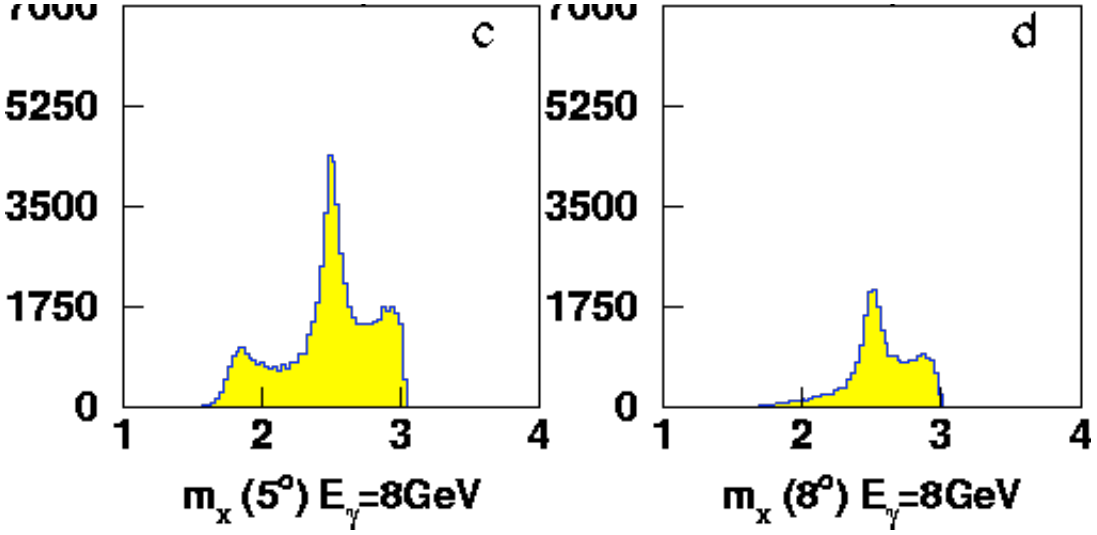

In Figure 4, the drop-out at low values of m_x are due two two things. First, the lower mass system is produced more forward, and at higher total momentum than a higher mass system. Second, when the decay $X \to \bar{K}^* K^*$ occurs, the Q value is very small. The K^* are essentially produced at rest in the rest frame of the X, or more importantly, with very small $p_\perp$ in the lab. When the K° subsequently decay, there is a larger probability that at least one of the daughters also will have very small $p_\perp$ in the lab. This leads to a larger probability that at least one of the final state charged particles is missed.

The drop-out at the highest values of m_x is due to the fact that the K^*'s have their maximum energy here. This decreases the maximum opening angle of the daughters, and increases the probability that at least one charged particle is in the forward region. This problem is most severe for the 12 *GeV* beam energy and the 8° hole, while for lower energies, and smaller holes, the high-end drop-off is much sharper. Additionally, in the highest mass system, the recoil proton tends to be more forward, (see section 0.1.5) and is likely to be missed.

Figure: The efficiency of the reconstruction of the $K^* \bar{K}^*$ mass as a function of beam energy (rows) and scattering angle θ. The vertical axis is the efficiency and the horizontal axis is the invariant mass of the $K^* \bar{K}^*$ system. **a** to **c** are for $E_\gamma = 6GeV$ with a 2°, 5° and 8° degree cut on θ respectively. **d** to **f** are for $E_\gamma = 8GeV$,**g** to **i** are for $E_\gamma = 10GeV$ and **j** to **l** are for $E_\gamma = 12GeV$. The apparent rise in efficiency at low mass is due to statistical fluctuations, it is not real.

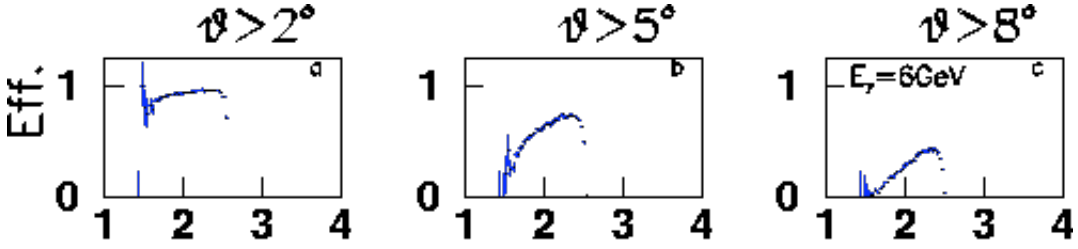

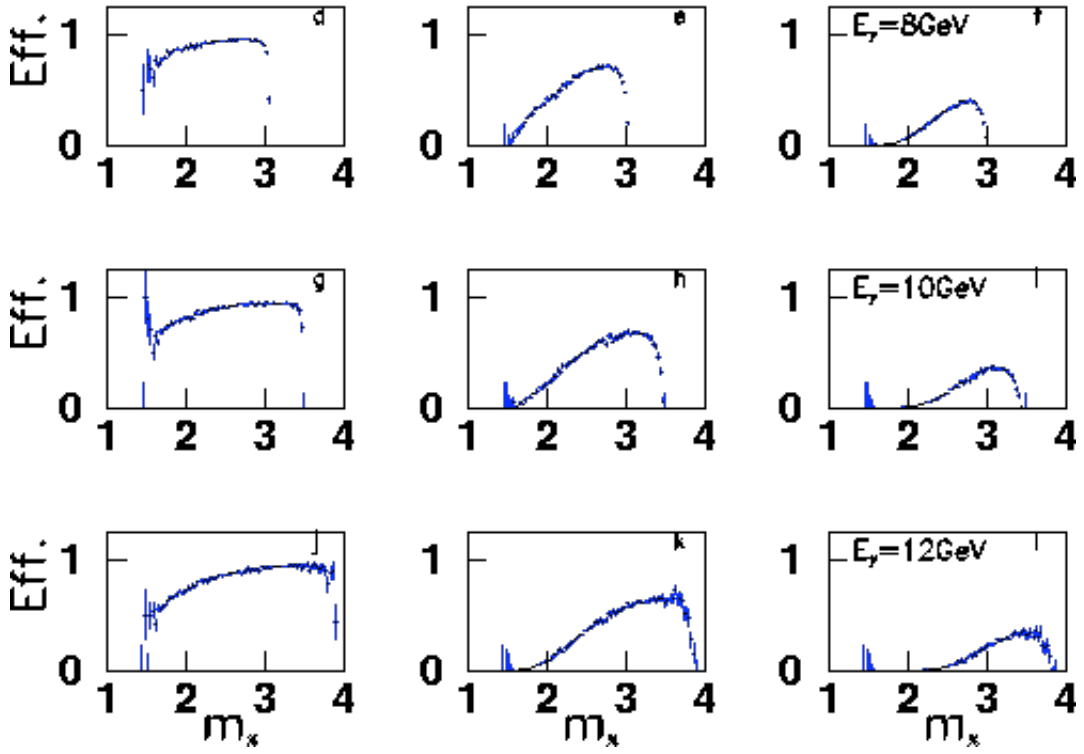

Similar to the missing mass, we have also examined the Godfreid-Jackson angle, θ_{GJ} for the $\bar{K}^*K^*$ system. In Figure 5 is plotted $\cos(\theta_{GJ})$ at $E_\gamma = 8GeV$ for three different scattering angle cuts. In Figure 6, we have formed the efficiency of measuring this quantity as a function of E_γ and the scattering angle cuts. This angle is very important in PWA analysis, as the distribution is directly related to the spin of the resonance. In doing PWA, one would like the acceptance in this quantity to be as large and as uniform as possible. In principle, if we understand this acceptance exactly, then PWA is always possible. In practice, there are always difficulties, and one wants the overall corrections to be as small as possible.

For this final state, Figure 6 shows that with a $\theta = 2^\circ$ cut, that we have reasonably high and uniform acceptances at all beam energies. As we go to the 5° cut, we see the rapid deterioration in acceptance as we go from $6GeV$ up to $12GeV$, (this cut corresponds to the solenoid-only mode in stage one). Finally, the 8° cut is painful at all beam energies, but is probably deadly at $8GeV$ and above.

Figure: The reconstructed $\cos(\theta_{GJ})$ for an $8GeV$ photon beam energy as a function of the most forward scattering angle.**a** is for all events, **b** is for θ larger than 2°, **c** is for θ larger than 5° and **d** is for θ large than 8°

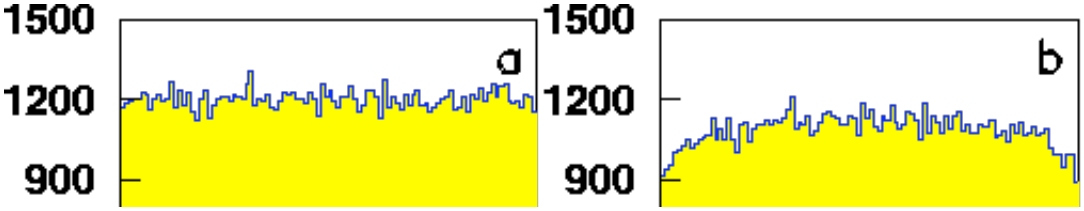

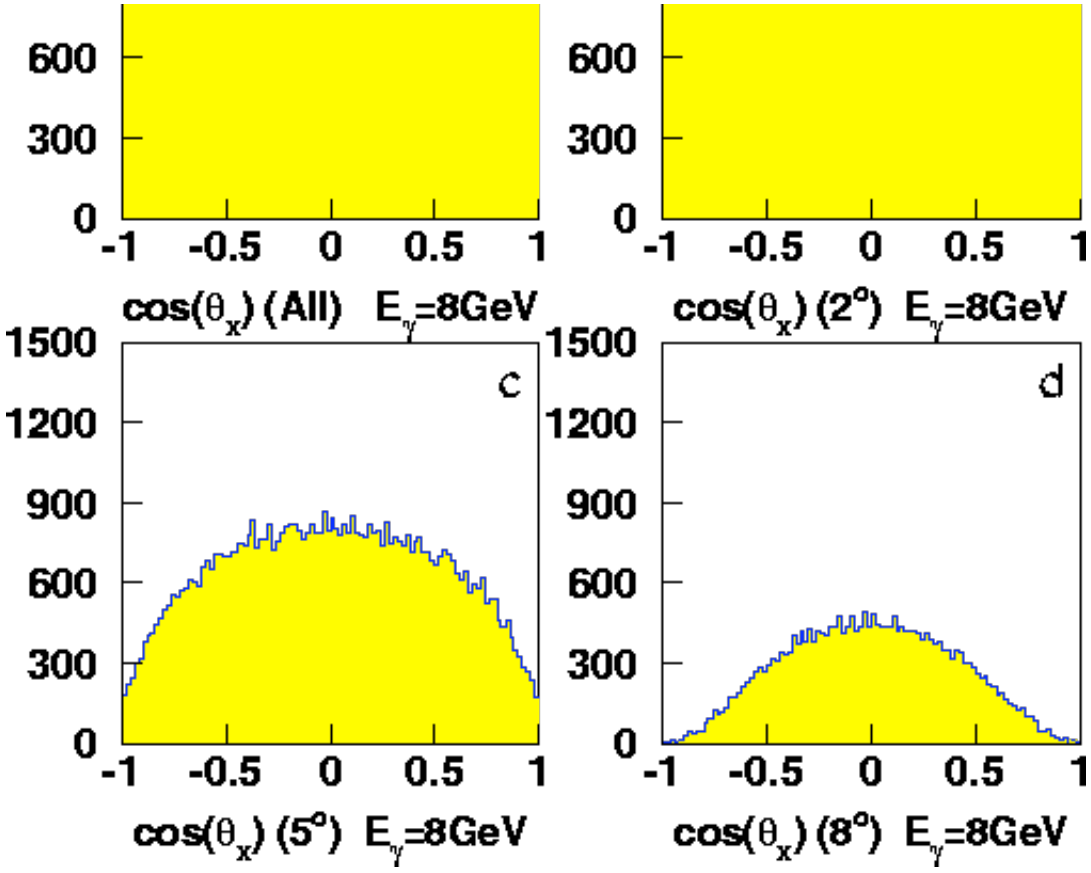

Figure: The efficiency of the reconstruction of the $\cos(\theta_{GJ})$ for the $K^*\bar{K}^*$ system as a function of beam energy (rows) and scattering angle θ. The vertical axis is the efficiency and the horizontal axis is $\cos(\theta_{GJ})$.**a** to **c** are for $E_\gamma = 6GeV$ with a 2°, 5° and 8° degree cut on θ respectively. **d** to **f** are for $E_\gamma = 8GeV$, **g** to **i** are for $E_\gamma = 10GeV$ and **j** to **l** are for $E_\gamma = 12GeV$.

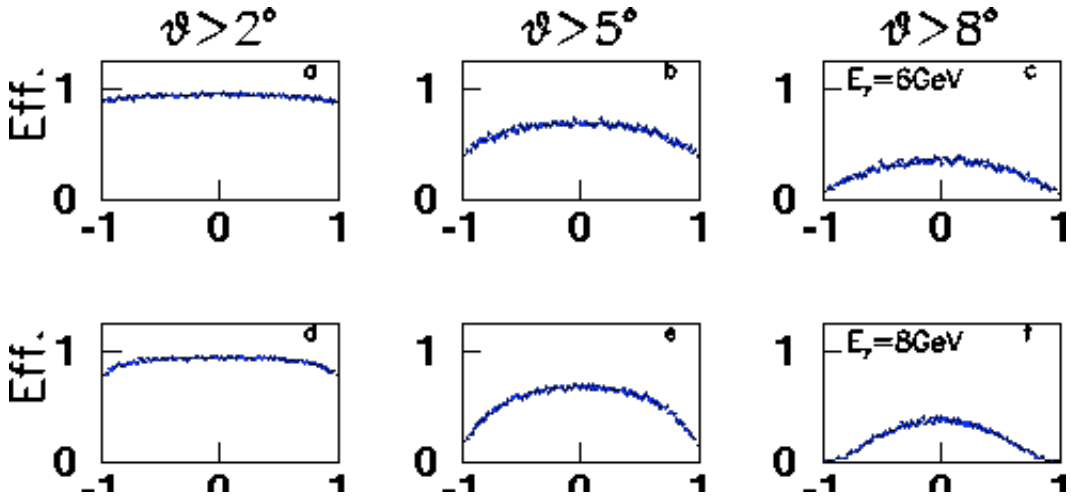

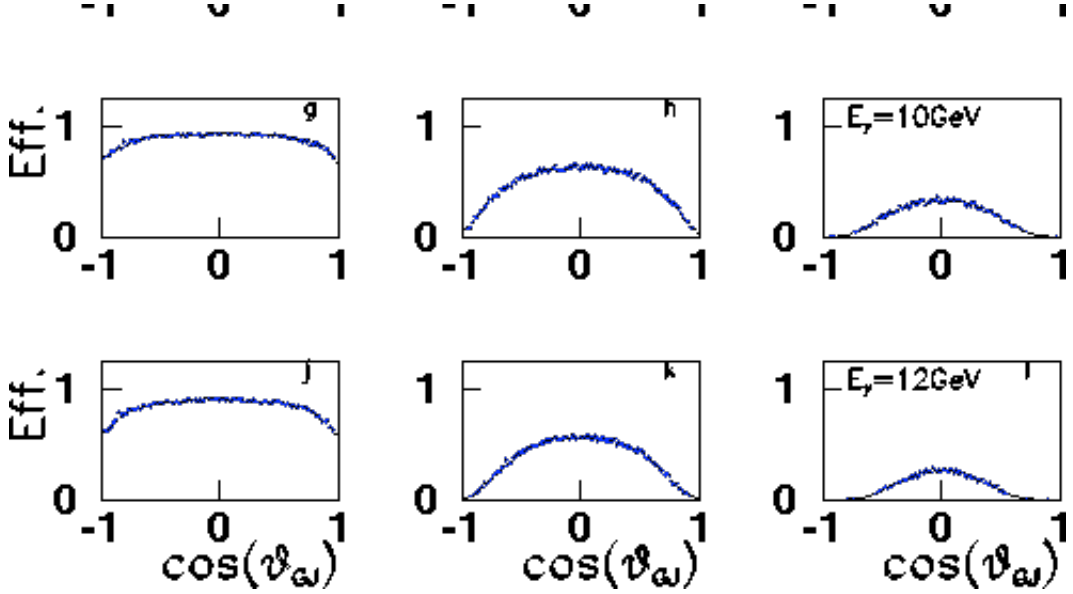

Recoil Proton Distributions

In Figure 7 we show the θ versus *p* distributions for the recoil proton in reaction 1. There are several features of merit in these plots. First, the band structure corresponds to the resonance structure in the $K^*\bar{K}^*$ system. This plot also reflects the *t* distribution, at higher E_γ , a given m_x can be produced at lower *t*, (see Figure 1). For all beam energies, the highest m_x corresponds to a very fast proton at small angles. By going to higher beam energies, the recoil proton for a fixed m_x is pulled to lower momentum and larger angles.

There is also a largest proton angle which increases as the beam energy is increased. However, this angle does not exceed 90° and for all cases shown her, it is smaller than 60° .Lastly, there is a minimum proton momentum which decreases as the beam energy is increased. For $E_\gamma = 6GeV$, it is approximately 350MeV/c, while at 12 GeV, it is about 150MeV/c. one important point is the radius of curvature of a track. $p_\perp = eBr$ which for r_{min}=0.3m we get $p_\perp = (0.3\frac{GeV/c}{Tm})(2.24T)(0.4m) = 0.201GeV/c$. Any values of $p_\perp$ smaller than this will curl around in the magnet. All tracks below the hyperbolic like cure on each track have a $p_\perp$ smaller than the critical value, and can in principal spiral in the 2.24T magnetic field. Based on the assumption that the particle needs to travel 3.65 meters in *z* to exit the magnet, we have indicated on the figure how many turns the proton will make. The small vertical lines below the hyperbolic curve are labeled $\frac{1}{2}$, 1, 2, 3 and 4. This is the number of turns which a track on that line will make. All tracks to the right of the line will make fewer turns, while all to the left of the line will make more. The conclusion from this is that for the highest energy beam, we are going to need to be able to identify the proton from tracking alone. The good news is that the momentum of these protons is in a range where dE/dx will work well.

Figure: The scattering angle θ versus the total momentum p for the recoil proton in reaction 1. The band structures correspond the the different resonances in the $\bar{K}^{*0}K^{*0}$ system. Protons below the curved line can in principal spiral in the magnetic field. The number of turns they make is indicated by the small vertical lines below the curved lines. Protons to the right of a line make fewer turns than labled on the line, those to the left make more.

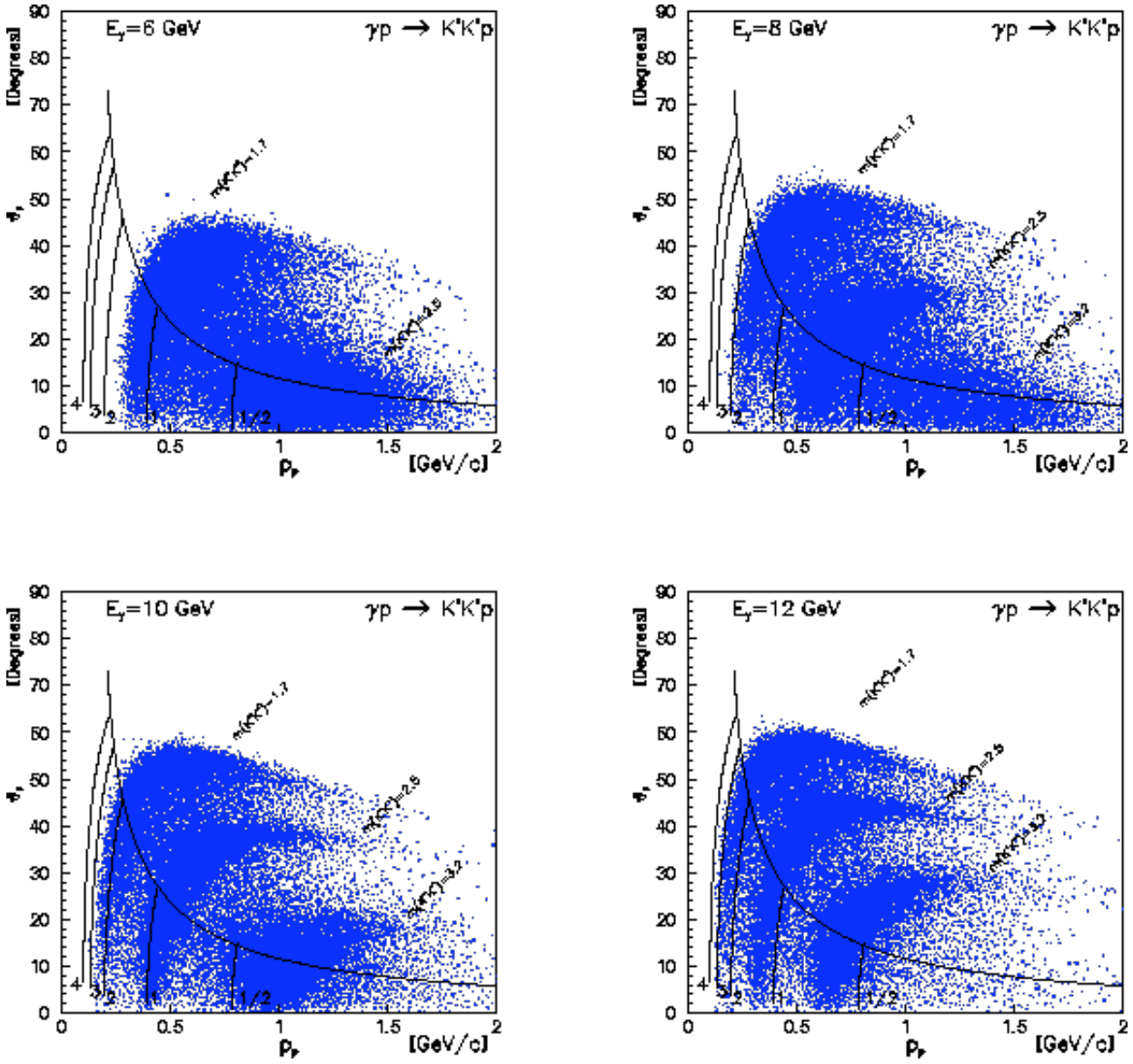

$p_\perp$ versus $p_{||}$ for K^+ and K^-

Of additional interest is to identify where the charged kaons are. In particular, where will we need particle identification, and what type will be sufficient to separate the kaons from pions and protons. In Figure 8 are plotted the transverse versus the longitudinal momentum for the charged kaons at the four beam energies. Indicated on each plot are various θ angles as seen in the lab. It should be noted that all tracks with $p_\perp$ smaller than 0.201 *GeV/c* can spiral in the 2.24 *T* magnetic field. This means that they may not reach a time-of-flight barrel. A time-of-flight measurement would require them to reach the detector system in front of the Pb-glass wall.

Of somewhat more relevance here is that most of the charged kaons are more forward than $\theta_K = 45°$, and at the lowest beam energy, very few are more forward than $\theta = 5°$.

Figure: The transverse versus longitudinal momentum for the K^+ and K^- from reaction 1. The lines indicate various scattering angles, θ as measured at the production vertex.

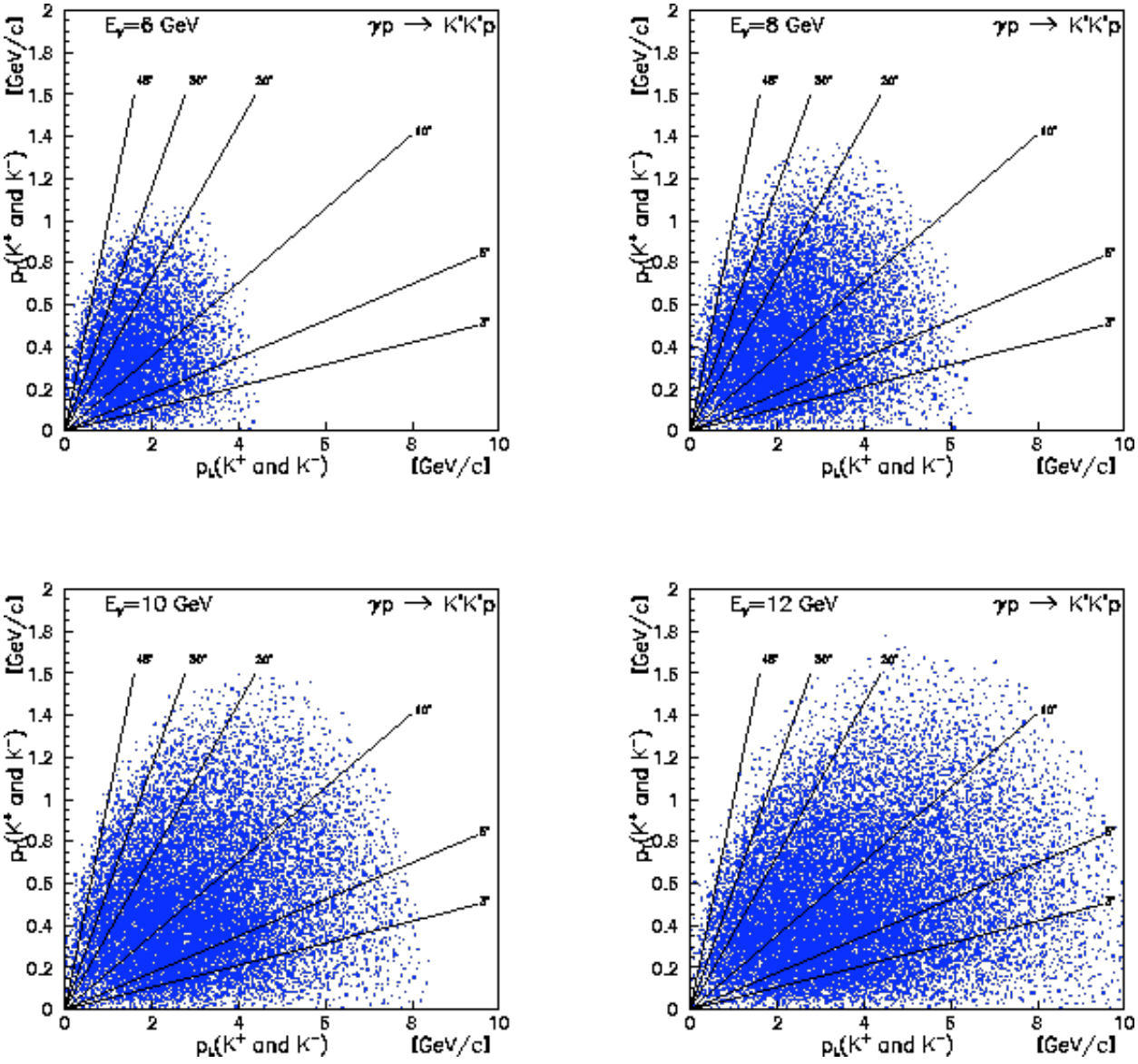

Curtis A. Meyer
5/29/1998